

# Synthesis, Characterization and *In-Vitro* Toxicity Assessment of Superparamagnetic Iron Oxide Nanoparticles for Biomedical Applications

Sivaranjani Sivalingam, Mahalakshmi Santhanakrishnan, Vijaya Parthasarathy✉  
Department of Nanoscience and Technology, Bharathiar University, Coimbatore, India

✉ Corresponding author. E-mail: vijayaparthasarathy@buc.edu.in

**Received:** Jul. 11, 2021; **Revised:** May 20, 2022; **Accepted:** Nov. 28, 2022; **Published:** Nov. 30, 2022

**Citation:** S. Sivalingam, M. Santhanakrishnan, V. Parthasarathy. Synthesis, characterization and *in-vitro* toxicity assessment of superparamagnetic iron oxide nanoparticles for biomedical applications. *Nano Biomedicine and Engineering*, 2022, 14(3): 201–207.

**DOI:** 10.5101/nbe.v14i3.p201–207

## Abstract

On the growing clinical demands, superparamagnetic iron oxide nanoparticles (SPIONs) have a vital role due to their infinite physical and chemical properties at the nanoscale. The researchers have started to focus more on the magnetite nanoparticle applications with unique shape and size in various filed such as biomedicine, food and environment to synthesize Fe<sub>3</sub>O<sub>4</sub> NP. Here we synthesized SPIONs-Fe<sub>3</sub>O<sub>4</sub> NP successfully by co-precipitation technique. The prepared nanoparticles were characterized using suitable analytical tools for structural, morphological, elemental, optical and thermogravimetric analysis. Moreover, the genotoxicity and hemolysis assay test has been carried out to estimate the toxicity of SPIONs-Fe<sub>3</sub>O<sub>4</sub> NP at various concentrations. The results found that 25 µg/mL concentration of SPIONs-Fe<sub>3</sub>O<sub>4</sub> NP shows good hemocompatibility than other concentrations. The genotoxicity assay was examined in *Allium cepa* (onion root tips) for chromosomal aberration. Hence, the present study discusses the synthesis characterization, assessing the genotoxicity and hemocompatibility potential for the synthesized Fe<sub>3</sub>O<sub>4</sub> NPs.

**Keywords:** Superparamagnetic iron oxide nanoparticles (SPIONs); Co-precipitation method; *Allium cepa* test; Hemolysis assay

## Introduction

The large number of research work on nanoparticles has resulted in significant advancements in various biomedical applications. The nanoscale materials such as silica, gold, silver, carbonaceous materials, Titanium, magnetic materials etc., have important biological applications like cancer therapeutics [1–10]. Especially, magnetic nanoparticles are at the foundation of nanotechnology-based structures, and they have made a significant difference in nanomedicine, analytical chemistry, electronics, and biosensing [11, 12]. Among

several magnetic nanoparticles such as Ni, Co, Fe, and their respective ferrite composition, Fe<sub>2</sub>O<sub>3</sub> and Fe<sub>3</sub>O<sub>4</sub> magnetic nanoparticles are the most prevalent. Extremely magnetic particles such as Co and Ni are responsive to oxidation and are harmful, whereas iron oxide nanoparticles and ferrites are most functional due to their low cytotoxicity and smaller size [12–14].

SPIONs are the most extensively used in nanomedicines application in either conventional or novel advancements. The activity of the Fe<sub>3</sub>O<sub>4</sub> nanoparticles strongly depends on their size, shape, including their crystal phase for its applications.

Various studies have been exposed that the shape has a great impact on the properties of  $\text{Fe}_3\text{O}_4$  nanoparticles for their potential applications [15, 16]. They are particularly developed for targeted drug delivery, clinical diagnosis, magnetic resonance imaging, bioremediation, hyperthermia, cancer biomarker due to their superior magnetic response property [12, 13]. Also, they demonstrate interesting properties such as high saturation field, superparamagnetism, high field irreversibility, and shifted loops after the field cooling. For these properties, the particles don't have an extensive demonstration of magnetic interrelation after the external magnetic field is detached [17]. In general, particles are made by minor crystals of iron oxides, normally called magnetite ( $\text{Fe}_3\text{O}_4$ ) or maghemite ( $\gamma\text{-Fe}_2\text{O}_3$ ) [18]. They are synthesized by various techniques, such as co-precipitation, sol-gel, hydrothermal, mixture, thermal decomposition, electrochemical and microemulsion synthesis. Among them, the co-precipitation method is the most effective, common and economical method for high-yield synthesis. Attributing to these advantages, the extensive particles size distribution of the subsequent mixture is synthesized by the co-precipitation technique [19-21].

In this research, we synthesized SPIONs- $\text{Fe}_3\text{O}_4$  NPs using coprecipitation method. Various characterization analyses were performed and the hemocompatibility of  $\text{Fe}_3\text{O}_4$  NPs was analyzed using human red blood cells (RBCs). Similarly, a genotoxic study was also performed using *Allium cepa* (onion root tips).

## Materials and Methods

### Materials

Ferric chloride tetrahydrate, Ferric chloride hexahydrate and Ammonia solution were procured from Himedia Laboratory Pvt. Ltd. All the used chemicals were used in research grade.

### Synthesis of iron oxide nanoparticles (co-precipitation method)

0.1 mol/L (30 mL) of ferric chloride hexahydrate and 0.1 mol/L (15 mL) of ferric chloride tetrahydrate were mixed well, and 3 mL of 5 mol/L ammonia solution was added dropwise and magnetically stirred continuously until a homogeneous solution was attained. Further, the stirring condition was maintained in a nitrogen-gas atmosphere. Finally, the obtained  $\text{Fe}_3\text{O}_4$  NP precipitate was washed three times by centrifugation (4000 r/min for 15 min at 87 °C), and the supernatant was removed [22]. The resultant

product was a pure – Iron oxide nanoparticles, which is shown as a schematic diagram in Fig. 1.

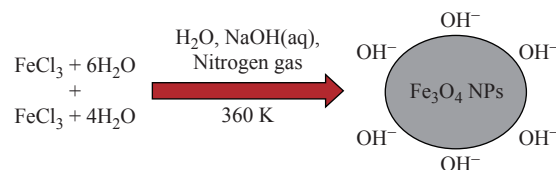


**Fig. 1** Schematic diagram for the synthesis of iron oxide nanoparticles by coprecipitation method

### Characterization techniques

To confirm the crystallinity of the prepared, the X-ray diffractometer (XRD) was carried out with Cu-K $\alpha$  radiation (1.5406 Å), the morphological analysis was studied with field emission scanning electron microscope (FESEM) (Quanta-250-FEG), the elemental composition was identified by elemental diffraction spectroscopy (EDS). The functional groups were confirmed by Fourier transformed Infrared (FTIR) spectroscopy (Bruker Tensor 27) with the range from 400  $\text{cm}^{-1}$  to 4000  $\text{cm}^{-1}$ . The thermal stability of the material was observed by thermogravimetric analysis (TGA) and STA 8000 (PerkinElmer), the in-vitro hemocompatibility was evaluated by UVvisible spectrophotometer (JoscoV-650, Japan).

### *Allium cepa* test

The genotoxicity effects of  $\text{Fe}_3\text{O}_4$  nanoparticles were performed by using *Allium cepa* to analyze the chromosomal aberration. The healthy onion bulbs with roots of about 2 to 3 cm were used with different concentrations of  $\text{Fe}_3\text{O}_4$  nanoparticles.  $\text{Fe}_3\text{O}_4$  NPs were exactly quit in the distilled water for various concentrations of control (25, 50, 75 and 100  $\mu\text{g}/\text{mL}$ , respectively) [23, 24].

### Hemolysis assay

To analyze the hemocompatibility of prepared  $\text{Fe}_3\text{O}_4$  NPs, a hemolysis assay test was carried out using a human blood cell sample. For this, 5 mL of blood was taken and centrifuged for 5 min at 6000 r/min to isolate the red blood cells from the blood sample. The red blood cell Pellet composed was diluted with 5 mL of PBS and centrifuged for 5 mins at 6000 r/min. Further, the 4 mL of  $\text{Fe}_3\text{O}_4$  NPs were dissolved with 1 mL of red blood cell diluted at 25, 50, 75 and 100  $\mu\text{g}/\text{mL}$  in phosphate buffered saline (PBS) solution and were incubated for 3 h at 36 °C. Subsequently, after 3 hrs, all the tubes were centrifuged at 6000 r/min for 15 min, and the performed supernatant result was gathered to

evaluate the UVvisible absorbance at a wavelength of 540 nm to estimate the haemoglobin release [25, 26].

## Result and Discussion

Table 1 exhibits various characterization techniques required to confirm the physiochemical properties of synthesized SPIONs-Fe<sub>3</sub>O<sub>4</sub> NPs and their respective outcomes obtained. The FESEM analysis confirmed that the morphology was cubic in nature, and the elements present were also confirmed with their atomic weight percentage by EDS analysis. The grain size of the SPIONs was calculated as 20 nm from XRD by using the Scherrer equation. But from the morphological observation, the particle size was measured as approximately 65 nm. The correlation of grain size calculation between the Scherrer equation and FESEM morphological scale measurement is different, and it may be negligible in range. The UVvisibleabsorption range of SPIONs was determined as 368 and 399 nm. From TGA analysis, the weight loss of Fe<sub>3</sub>O<sub>4</sub> NPs was observed at about 800 °C, and nearly 70% of the iron oxide was found to be stable [27].

### XRD analysis

Figure 2 shows the XRD pattern for synthesized Fe<sub>3</sub>O<sub>4</sub>NPs, where main peaks are placed at 30.07°, 35.42°, 43.04°, 53.40°, 57.42° and 63.53° which correspond to (220), (311), (400), (422), (511) and (440), showing a cubic crystalline structure. To verify the crystalline magnetite structure of the synthesized

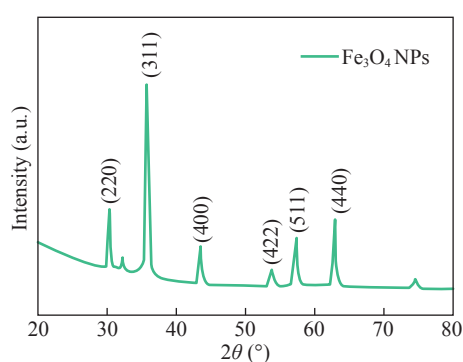


Fig. 2 XRD pattern of Fe<sub>3</sub>O<sub>4</sub> NPs

Fe<sub>3</sub>O<sub>4</sub> nanoparticles, XRD analysis was performed with a scan from 20°–80° with a step size of 2° per minute. The analyzed diffraction peak positions with parallel plane orientations of Fe<sub>3</sub>O<sub>4</sub> nanoparticles approve with the standard data (JCPDS Card No: 89-0950). The grain size (*D*) for the Fe<sub>3</sub>O<sub>4</sub> nanoparticles were evaluated by applying the Scherrer formula:

$$D = n\lambda/(\beta\cos\theta), \quad (1)$$

where *n* is the integer,  $\lambda$  is the wavelength of the incident X-ray,  $\beta$  is the full width half maximum and  $\theta$  is the Bragg angle.

The calculated grain size for Fe<sub>3</sub>O<sub>4</sub> nanoparticles is 20 nm [28].

### Field emission scanning electron microscopy (FESEM) analysis

The FESEM images of Fe<sub>3</sub>O<sub>4</sub> nanoparticles are viewed at 2 μm and 500 nm magnification (Fig. 3), and a cubic-shaped morphology was observed. This may be attributed to the incorporation of ammonia and the presence of nitrogen during the synthesis procedure. They have a few graininess structures, which are

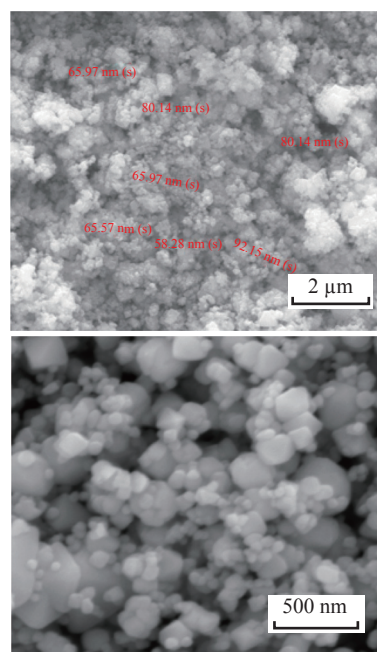


Fig. 3 FESEM image of Fe<sub>3</sub>O<sub>4</sub> NPs

Table 1 Characterization techniques of superparamagnetic iron oxide nanoparticles

Characterization of Superparamagnetic iron oxide nanoparticles (SPIONs)						
No.	Particles	FESEM (morphology)	EDS (elements)	UVvisible spectroscopy (absorbance range)	XRD (grain size)	TGA (weight loss percentage)
1	Fe <sub>3</sub> O <sub>4</sub> -NPs	Cube shaped; particle size in ~65nm	w(Fe) = 61.72% w(O) = 38.28%	368 and 399 nm	20 nm	70% stability

very small particles of the cube structure of  $\text{Fe}_3\text{O}_4$  nanoparticles [29].

### EDS analysis

The energy dispersive X-ray spectroscopy (EDS) was analyzed to confirm the elements present in the  $\text{Fe}_3\text{O}_4$  nanoparticles. As shown in Fig. 4, the weight percentage of Fe and O are present at 61.72% and 38.28%, respectively [30].

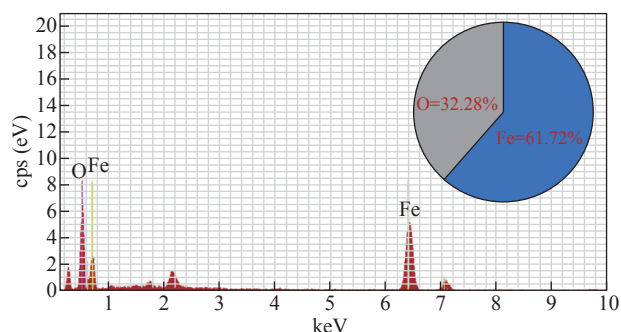


Fig. 4 EDS spectra of  $\text{Fe}_3\text{O}_4$  NPs

### UV visible spectroscopy analysis

In the UV visible spectroscopy analysis (Fig. 5), the absorption peak hump for  $\text{Fe}_3\text{O}_4$  nanoparticle was found in 360–420 nm UV range. However, the minute sharp peak at 368 nm and 399 nm correspond to the oxide group present in the  $\text{Fe}_3\text{O}_4$  NPs and the magnetite presence. In this way, UV-Visible analysis further confirmed the formation of  $\text{Fe}_3\text{O}_4$  nanoparticle [31].

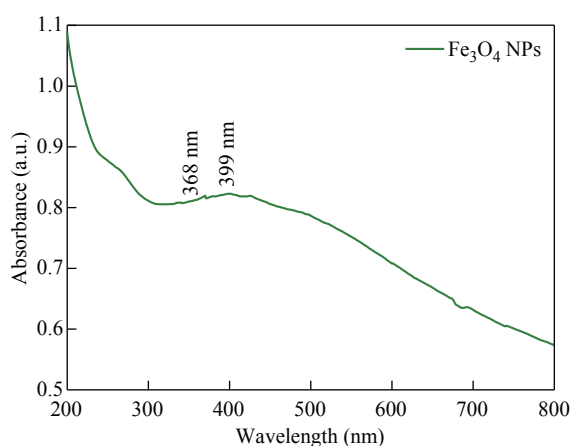


Fig. 5 UV visible Spectrum of  $\text{Fe}_3\text{O}_4$  NPs

### FTIR analysis

The functional group confirmation for synthesized  $\text{Fe}_3\text{O}_4$  NPs was revealed by FTIR analysis which is shown in Fig. 6. The strong absorption band at 622  $\text{cm}^{-1}$  and 583  $\text{cm}^{-1}$  shows the formation of magnetic

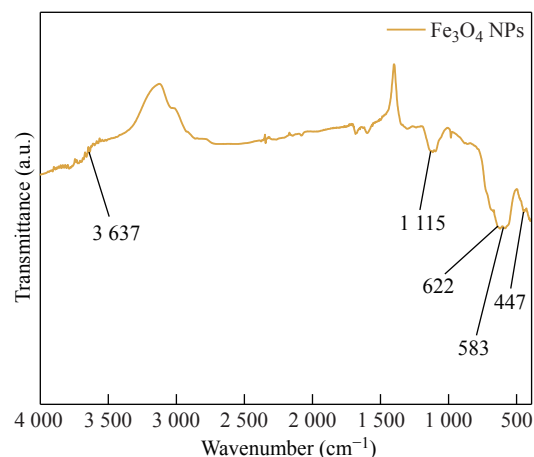


Fig. 6 FTIR spectrum of synthesized  $\text{Fe}_3\text{O}_4$  NP

nanoparticles. The stretching vibration of tetrahedral sites of spinel structure of Fe—O was confirmed at 583  $\text{cm}^{-1}$ . The band at 447  $\text{cm}^{-1}$  is attributed to octahedral and tetrahedral sites; also, the peak at 3637  $\text{cm}^{-1}$  corresponds to the O—H stretching on the surface of the  $\text{Fe}_3\text{O}_4$  NPs.

### TGA analysis

The thermal stability of the synthesized  $\text{Fe}_3\text{O}_4$  NPs was analyzed by TGA analysis under nitrogen atmosphere at the heating rate of 10  $^{\circ}\text{C}/\text{min}$ . As exhibited in Fig. 7. The removal of physically trapped water molecules caused the initial mass loss of around 3% at temperatures below 200  $^{\circ}\text{C}$ , and the thermal degradation of the organic parts grafted on the surface of the nano-catalyst caused the second mass loss in the temperature range of 200–600  $^{\circ}\text{C}$ . Further, the weight loss of  $\text{Fe}_3\text{O}_4$  NPs was nearly 30% at 800  $^{\circ}\text{C}$ , which was due to the volatilization of the water. This proves that 70% of the iron oxide has thermal stability [32].

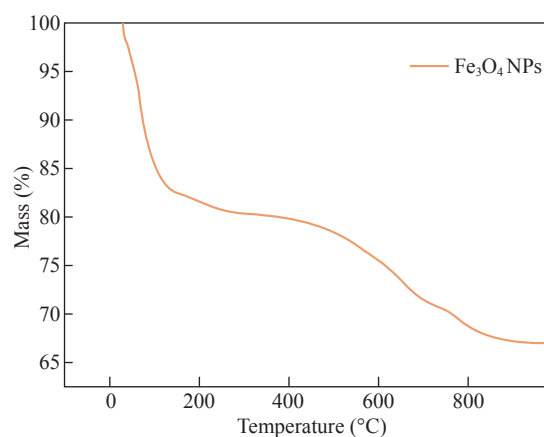
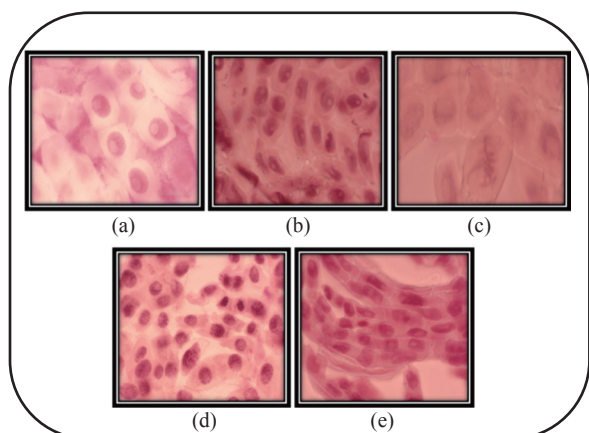


Fig. 7 TGA analysis of  $\text{Fe}_3\text{O}_4$  NPs

### Chromosomal aberrations assay

The genotoxic effect of  $\text{Fe}_3\text{O}_4$  NPs is studied in the



**Fig. 8** Different types of mitosis phases in *Allium cepa*. (a) Interphase; (b) Prophase; (c) Sticky metaphase; (d) Anaphase; and (e) Telophase seen in tip of *Allium cepa* after 12 h incubation with  $\text{Fe}_3\text{O}_4$  NPs

root tips of *Allium cepa*. From the optical microscopy analysis, the results were comprehensive for the various concentrations of  $\text{Fe}_3\text{O}_4$  NPs. As shown in Fig. 8, the several mitosis phases, specifically the prophase and interphase of the exposed chromosomes, are quite evidently seen and are individual of the phase at control, i.e., 25  $\mu\text{g}/\text{mL}$ . The sticky metaphase showed chromosomes aberration at 50  $\mu\text{g}/\text{mL}$ , and the anaphase showed chromosomes development to opposite poles in an even way at 75  $\mu\text{g}/\text{mL}$  [33]. The telophase stage in which the chromosomes were prepared at opposite poles, waiting for cytokines was observed at 100  $\mu\text{g}/\text{mL}$  respectively.

### **In-vitro hemocompatibility assay**

A hemolysis assay was executed to analyze the hemocompatibility for the prepared  $\text{Fe}_3\text{O}_4$  using human red blood cells with series of  $\text{Fe}_3\text{O}_4$  concentrations such as 25, 50, 75 and 100  $\mu\text{g}/\text{mL}$ . From the outcomes, as shown in Fig. 9,  $\text{Fe}_3\text{O}_4$  nanoparticles showed propagated hemolytic results based on increasing concentration, evaluated on the human RBCs. From the statistical analysis, the significant error was shown as  $< 0.05$ , which is relatively considered. The low-level concentration of  $\text{Fe}_3\text{O}_4$  25  $\mu\text{g}/\text{mL}$  shows better results compared with higher concentrations (100  $\mu\text{g}/\text{mL}$ ). The reason for the above results is due to the erythrocytes level on the blood may be damaged and enhance the free haemoglobin level, leading to reduce the transport of oxygen to the tissues. Our research resolved that  $\text{Fe}_3\text{O}_4$  NPs are non-hemolytic at lower concentrations against human RBCs, confirming biocompatibility and non-hazardous nature of  $\text{Fe}_3\text{O}_4$  NPs.

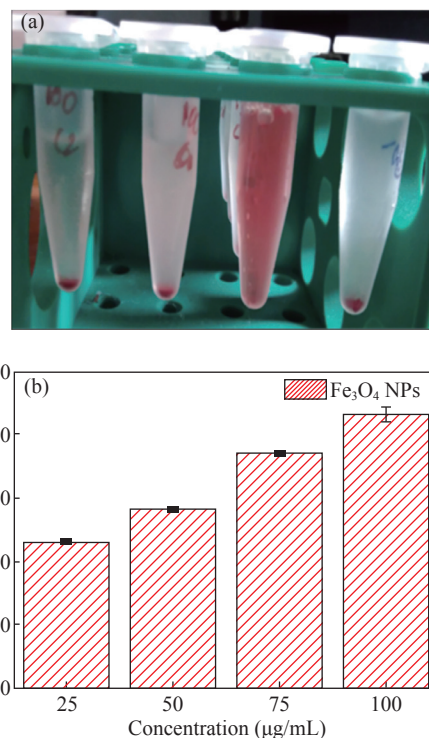


**Fig. 9** (a) Hemolysis image; (b) Hemolysis activity of  $\text{Fe}_3\text{O}_4$  NPs

## **Conclusion**

The superparamagnetic iron oxide nanoparticles (SPIONs) were synthesized by the facile coprecipitation technique. The XRD and FESEM studies confirmed the formation of grain size and morphology. Adopting the Scherrer equation, the grain size was found to be 20 nm, and a cubic morphology was observed by FESEM analysis. The coherence proportion of Fe and O elements present in the  $\text{Fe}_3\text{O}_4$  NP was identified by EDS analysis. The UV visible absorption peak for  $\text{Fe}_3\text{O}_4$  NPs was observed at 360 nm. The thermal stability of the SPIONs was analyzed by thermogravimetric analysis. The chromosomal aberration was analyzed by using the *Allium cepa* root tip. From the hemocompatibility analysis, the toxic level for the synthesized  $\text{Fe}_3\text{O}_4$  NP was analyzed. The mitotic index marker of increasing and decreasing the cells through mitosis for genotoxicity effects indicated that the synthesized  $\text{Fe}_3\text{O}_4$  NPs are the potential transporter of chromosomal aberration. Furthermore, the hemocompatibility for the  $\text{Fe}_3\text{O}_4$  NPs towards human RBCs was observed from lower to higher concentrations and confirmed that the lower concentration level of 25  $\mu\text{g}/\text{mL}$   $\text{Fe}_3\text{O}_4$  NPs is hemocompatible. Here we concluded that the synthesized superparamagnetic iron oxide nanoparticles are a promising material for biomedical

applications.

## Acknowledgements

The authors are grateful to DST-FIST and UGC SAP, New Delhi, India for the instrumentation facilities. Funding was provided by the RUSA 2.0 – BEICH Government of India and Department of Science and Technology (DST) PURSE-Phase-II.

## Conflict of Interests

The authors declare no conflict of interest to the manuscript.

## Reference

- [1] L. Mahendran, A. Ravichandran, A.M. Ballamurugan. Organic and inorganic template-assisted synthesis of silica nanotubes and evaluation of their properties. *Applied Biochemistry and Biotechnology*, 2022, 194: 167–175. <http://dx.doi.org/10.1007/s12010-021-03740-4>
- [2] M. Jabir, U.I. Sahib, Z. Taqi, et al. Linalool-loaded glutathione-modified gold nanoparticles conjugated with CALNN peptide as apoptosis inducer and NF- $\kappa$ B translocation inhibitor in SKOV-3 cell line. *International Journal of Nanomedicine*, 2020, 15: 9025–9047. <https://doi.org/10.2147/ijn.s276714>
- [3] M.S. Jabir, Y.M. Saleh, G.M. Sulaiman, et al. Green synthesis of silver nanoparticles using *Annona muricata* extract as an inducer of apoptosis in cancer cells and inhibitor for NLRP3 inflammasome via enhanced autophagy. *Nanomaterials*, 2021, 11: 384. <https://doi.org/10.3390/nano11020384>
- [4] M.S. Jabir, A.A. Hussien, G.M. Sulaiman, et al. Green synthesis of silver nanoparticles from *Eriobotrya japonica* extract: A promising approach against cancer cells proliferation, inflammation, allergic disorders and phagocytosis induction. *Artificial Cells, Nanomedicine, and Biotechnology*, 2021, 49: 48–60. <http://dx.doi.org/10.1080/21691401.2020.1867152>
- [5] M. Logesh, A. Marimuthu, A.M. Ballamurugan. Fabrication of graphene incorporated biphasic calcium phosphate composite and evaluation of impact of graphene in the in-vitro biomineralization process. *Materials Chemistry and Physics*, 2019, 232: 75–81. <https://doi.org/10.1016/j.matchemphys.2019.04.049>
- [6] S. Sivalingam, A. Kunhilitakath, P. Nagamony, et al. Fabrication, toxicity and biocompatibility of *Sesamum indicum* infused graphene oxide nanofiber - a novel green composite method. *Applied Nanoscience*, 2021, 11: 679–686. <http://dx.doi.org/10.1007/s13204-020-01596-4>
- [7] K.S. Khashan, F.A. Abdulameer, M.S. Jabir, et al. Anticancer activity and toxicity of carbon nanoparticles produced by pulsed laser ablation of graphite in water. *Advances in Natural Sciences: Nanoscience and Nanotechnology*, 2020, 11: 035010. <https://doi.org/10.1088/2043-6254/aba1de>
- [8] H.H. Bahjat, R.A. Ismail, G.M. Sulaiman, et al. Magnetic field-assisted laser ablation of titanium dioxide nanoparticles in water for anti-bacterial applications. *Journal of Inorganic and Organometallic Polymers and Materials*, 2021, 31: 3649–3656. <http://dx.doi.org/10.1007/s10904-021-01973-8>
- [9] S.H. Kareem, A.M. Naji, Z.J. Taqi, et al. Polyvinylpyrrolidone loaded-MnZnFe<sub>2</sub>O<sub>4</sub> magnetic nanocomposites induce apoptosis in cancer cells through mitochondrial damage and P<sup>53</sup> pathway. *Journal of Inorganic and Organometallic Polymers and Materials*, 2020, 30: 5009–5023. <http://dx.doi.org/10.1007/s10904-020-01651-1>
- [10] M.S. Jabir, U.M. Nayef, W.K. Abdulkadhim, et al. Fe<sub>3</sub>O<sub>4</sub> nanoparticles capped with PEG induce apoptosis in breast cancer AMJ13 cells via mitochondrial damage and reduction of NF- $\kappa$ B translocation. *Journal of Inorganic and Organometallic Polymers and Materials*, 2021, 31: 1241–1259. <http://dx.doi.org/10.1007/s10904-020-01791-4>
- [11] S. Al-Musawi, S. Albukhaty, H. Al-Karagoly, et al. Dextran-coated superparamagnetic nanoparticles modified with folate for targeted drug delivery of camptothecin. *Advances in Natural Sciences: Nanoscience and Nanotechnology*, 2020, 11: 045009. <https://doi.org/10.1088/2043-6254/abc75b>
- [12] J.R. Sosa-Acosta, C. Iriarte-Mesa, G.A. Ortega, et al. DNA-iron oxide nanoparticles conjugates: Functional magnetic nanoplatforms in biomedical applications. *Topics in Current Chemistry*, 2020, 378: 13. <http://dx.doi.org/10.1007/s41061-019-0277-9>
- [13] Y.F. Xiao, J.Z. Du. Superparamagnetic nanoparticles for biomedical applications. *Journal of Materials Chemistry B*, 2020, 8: 354–367. <https://doi.org/10.1039/c9tb01955c>
- [14] K. Raghava Reddy, P.A. Reddy, C.V. Reddy, et al. Functionalized magnetic nanoparticles/biopolymer hybrids: Synthesis methods, properties and biomedical applications. *Methods in microbiology*. Amsterdam: Elsevier, 2019: 227–254. <https://doi.org/10.1016/bs.mim.2019.04.005>
- [15] C.H. Li, R.X. Wei, Y.M. Xu, et al. Synthesis of hexagonal and triangular Fe<sub>3</sub>O<sub>4</sub> nanosheets via seed-mediated solvothermal growth. *Nano Research*, 2014, 7: 536–543. <http://dx.doi.org/10.1007/s12274-014-0421-3>
- [16] Z.I. Takai, M.K. Mustafa, S. Asman, et al. Preparation and characterization of magnetite (Fe<sub>3</sub>O<sub>4</sub>) nanoparticles by sol-gel method. *International Journal of Nanoelectronics and Materials*, 2019, 12: 37–46.
- [17] Morteza, Mahmoudi. Superparamagnetic iron oxide nanoparticles (SPIONs): Development, surface modification and applications in chemotherapy. *Advanced Drug Delivery Reviews*, 2011, 63: 24–46. <http://dx.doi.org/10.1016/j.addr.2010.05.006>
- [18] J. Dulińska-Litewka, A. Łazarczyk, P. Hałubiec, et al. Superparamagnetic iron oxide nanoparticles-current and prospective medical applications. *Materials (Basel)*, 2019, 12: 617. <https://doi.org/10.3390/ma12040617>
- [19] S.M. Dadfar, D. Camozzi, M. Darguzyte, et al. Size-isolation of superparamagnetic iron oxide nanoparticles improves MRI, MPI and hyperthermia performance. *Journal of Nanobiotechnology*, 2020, 18: 22. <https://doi.org/10.1186/s12951-020-0580-1>
- [20] Ş.Y. Kaygisiz, İ.H. Cigerci. Genotoxic evaluation of different sizes of iron oxide nanoparticles and ionic form by SMART, *Allium* and comet assay. *Toxicology and Industrial Health*, 2017, 33: 802–809. <https://doi.org/10.1177/0748233717722907>
- [21] T. Liu, R. Bai, H.G. Zhou, et al. The effect of size and surface ligands of iron oxide nanoparticles on blood compatibility. *RSC Advances*, 2020, 10: 7559–7569. <http://dx.doi.org/10.1039/C9RA10969B>
- [22] P.L. Hariani, M. Faizal, R. Ridwan, et al. Synthesis and properties of Fe<sub>3</sub>O<sub>4</sub> nanoparticles by Co-precipitation method to removal procion dye. *International Journal of Environmental Science and Development*, 2013: 336–340. <https://doi.org/10.7763/ijesd.2013.v4.366>

- [23] O.M. Fadoju, O.A. Osinowo, O.I. Ogunsuyi, et al. Interaction of titanium dioxide and zinc oxide nanoparticles induced cytogenotoxicity in *Allium cepa*. *Nucleus*, 2020, 63: 159–166. <http://dx.doi.org/10.1007/s13237-020-00308-1>
- [24] P.S. Shiva Prasad, W.J. Kamal, F.J. Xavier, et al. Studies on the effect of zerovalent iron nanoparticles on allium cepa root tips. *International Journal of Research and Analytical Reviews*, 2020, 7(2): 855–859.
- [25] S. Mahalakshmi, N. Hema, P.P. Vijaya. *In vitro* biocompatibility and antimicrobial activities of zinc oxide nanoparticles (ZnO NPs) prepared by chemical and green synthetic route — a comparative study. *Bio Nano Science*, 2020, 10: 112–121. <http://dx.doi.org/10.1007/s12668-019-00698-w>
- [26] S. Mahalakshmi, P. Vijaya. Evaluation of *In-vitro* biocompatibility and antimicrobial activities of titanium dioxide (TiO<sub>2</sub>) nanoparticles by hydrothermal method. *Nano Biomedicine and Engineering*, 2021, 13: 36–43. <https://doi.org/10.5101/nbe.v13i1.p36-43>
- [27] R. Liman, B. Başbuğ, M.M. Ali, et al. Cytotoxic and genotoxic assessment of tungsten oxide nanoparticles in *Allium cepa* cells by *Allium*-telophase and comet assays. *Journal of Applied Genetics*, 2021, 62: 85–92. <http://dx.doi.org/10.1007/s13353-020-00608-x>
- [28] Y.P. Yew, K. Shameli, M. Miyake, et al. Green synthesis of magnetite (Fe<sub>3</sub>O<sub>4</sub>) nanoparticles using seaweed (*Kappaphycusalvarezii*) extract. *Nanoscale Research Letters*, 2016, 11: 276. <http://dx.doi.org/10.1186/s11671-016-1498-2>
- [29] V.K. Yadav, D. Ali, S.H. Khan, et al. Synthesis and characterization of amorphous iron oxide nanoparticles by the sonochemical method and their application for the remediation of heavy metals from wastewater. *Nanomaterials*, 2020, 10: 1551. <https://doi.org/10.3390/nano10081551>
- [30] R. Abhinayaa, G. Jeevitha, D. Mangalaraj, et al. Cytotoxic consequences of Halloysite nanotube/iron oxide nanocomposite and iron oxide nanoparticles upon interaction with bacterial, non-cancerous and cancerous cells. *Colloids and Surfaces B: Biointerfaces*, 2018, 169: 395–403. <https://doi.org/10.1016/j.colsurfb.2018.05.040>
- [31] N. Belachew, A. Tadesse, M.H. Kahsay, et al. Synthesis of amino acid functionalized Fe<sub>3</sub>O<sub>4</sub> nanoparticles for adsorptive removal of Rhodamine B. *Applied Water Science*, 2021, 11: 33. <http://dx.doi.org/10.1007/s13201-021-01371-y>
- [32] Q. Wu, F.L. Jiao, F.Y. Gao, et al. Development and application of immobilized surfactant in mass spectrometry-based proteomics. *RSC Advances*, 2017, 7: 44282–44288. <http://dx.doi.org/10.1039/C7RA08874D>
- [33] I.H. Ali, M.S. Jabir, H.S.A. Al-Shmgani, et al. Pathological And Immunological Study On Infection With *Escherichia Coli* in ale BALB/c mice. *Journal of Physics: Conference Series*, 2018, 1003: 012009. <https://doi.org/10.1088/1742-6596/1003/1/012009>

**Copyright**© Sivaranjani Sivalingam, Mahalakshmi Santhana-krishnan and Vijaya Parthasarathy. This is an open-access article distributed under the terms of the Creative Commons Attribution License (CC BY), which permits unrestricted use, distribution, and reproduction in any medium, provided the original author and source are credited.